

# 1 **Are microseismic ground displacements a significant geomorphic agent?**

2 Matthew J. Brain<sup>1</sup>, Nicholas J. Rosser, Emma C. Norman and David N. Petley

3 Department of Geography, Durham University, Science Site, South Road, Durham, DH1  
4 3LE, UK

## 5 **Abstract**

6 This paper considers the role that microseismic ground displacements may play in fracturing  
7 rock via cyclic loading and subcritical crack growth. Using a coastal rock cliff as a case  
8 study, we firstly undertake a literature review to define the spatial locations that may be prone  
9 to microseismic damage. It is suggested that microseismic weakening of rock can only occur  
10 in ‘damage accumulation zones’ of limited spatial extent. Stress concentrations resulting from  
11 cliff height, slope angle and surface morphology may nucleate and propagate a sufficiently  
12 dense population of microcracks that can then be exploited by microseismic cyclic loading.  
13 We subsequently examine a 32-day microseismic dataset obtained from a coastal cliff-top  
14 location at Staithes, UK. The dataset demonstrates that microseismic ground displacements  
15 display low peak amplitudes that are punctuated by periods of greater displacement during  
16 storm conditions. Microseismic displacements generally display limited preferential  
17 directivity, though we observe rarely occurring sustained ground motions with a cliff-normal  
18 component during storm events. High magnitude displacements and infrequently experienced  
19 ground motion directions may be more damaging than the more frequently occurring,  
20 reduced magnitude displacements characteristic of periods of relative quiescence. As high  
21 magnitude, low frequency events exceed and then increase the damage threshold, these  
22 extremes may also render intervening, reduced magnitude microseismic displacements  
23 ineffective in terms of damage accumulation as a result of crack tip blunting and the

24 generation of residual compressive stresses that close microcracks. We contend that damage  
25 resulting from microseismic ground motion may be episodic, rather than being continuous  
26 and in (quasi-)proportional and cumulative response to environmental forcing. A conceptual  
27 model is proposed that describes when and where microseismic ground motions can operate  
28 effectively. We hypothesise that there are significant spatial and temporal limitations on  
29 effective microseismic damage accumulation, such that the net efficacy of microseismic  
30 ground motions in preparing rock for fracture, and hence in enhancing erosion, may be  
31 considerably lower than previously suggested in locations where high magnitude  
32 displacements punctuate ‘standard’ displacement conditions. Determining and measuring the  
33 exact effects of microseismic ground displacement on damage accumulation and as a trigger  
34 to macro-scale fracture in the field is not currently possible, though our model remains  
35 consistent with field observations and conceptual models of controls on rockfall activity.

36 **Keywords:** rock slope; microseismicity; displacement; strain; stress; damage; rockfall

## 37 **1. Introduction and scope**

38 Microseismic monitoring techniques have recently been used to detect and characterise a  
39 range of geomorphic processes, including ocean wave energy delivery to coastal cliffs  
40 (Adams et al., 2002; Young et al., 2011; 2012 ; Dickson and Pentney, 2012), river bedload  
41 transport (Hsu et al., 2011; Tsai et al., 2012), glacier fracture and hydrology (Roux et al.,  
42 2008; West et al., 2010) and rock sliding and avalanching (Deparis et al., 2008; Dammeier et  
43 al., 2011). Whilst microseismicity has been used in these studies as a remote proxy for  
44 process, Adams et al. (2005) hypothesised that microseismic ground motions may themselves  
45 constitute a significant yet largely unrecognised geomorphic process that is worthy of further  
46 attention.

47 Adams et al. (2005) reported an exponential decay in the magnitude of micron-scale ( $0.1 - 1$   
48  $\times 10^1 \mu\text{m}$ ) displacements along a transect perpendicular to the face of a coastal rock cliff at  
49 Monterey Bay, California, USA. By comparison with ocean wave data, Adams et al. (2005)  
50 demonstrated that the observed flexure results from the loading of the foreshore platform by  
51 water waves, notably longer-period incident sea swell ocean waves (10 – 20 s period).  
52 Similar observations were also made by Young et al. (2011; 2012) at infragravity frequencies  
53 (20 – 170 s period). Adams et al. (2005) suggested that the low magnitude (micron-scale)  
54 cyclic nature of cliff-top microseismic ground displacements may be sufficient to damage the  
55 rock mass via a fatigue process, such that overall rock mass strength is progressively reduced  
56 as microcracks propagate, interact and coalesce (Attewell and Farmer, 1973; Main et al.,  
57 1993). If microseismic ground motions are significant in reducing rock mass strength, macro-  
58 scale rock fracture could therefore occur at ambient deviatoric stresses that are considerably  
59 less than the peak strength values of intact (undamaged) rocks (Sunamura, 1992; Xiao et al.,  
60 2011). Under this model, by creating planes of weakness, microseismic fatigue could play a  
61 key role in governing the timing and distribution of landform and landscape susceptibility to  
62 change (cf. Allison, 1996; Molnar et al., 2007; Moore et al., 2009; Dühnforth et al., 2010;  
63 Clarke and Burbank 2010; 2011; Koons et al., 2012). If microseismic cyclic loading is  
64 effective in weakening rocks in an incremental, preparatory manner and, hence, permitting  
65 fracture to occur more readily, this may be an important yet rarely considered process in  
66 driving slope failure.

67 As a preparatory geomorphic process (cf. Gunzberger et al., 2005), microseismic cyclic  
68 loading theoretically relies on an extremely high number of effective (damaging) load cycles  
69 to exert any significant geomorphic consequence, since the damage increment resulting from  
70 each loading cycle is likely to be exceedingly small, yet not cumulatively negligible (Adams

71 et al., 2005). For this to occur to a degree sufficient to be comparable to other damage-  
72 inducing processes, the spatial and temporal opportunity for microseismic damage must be  
73 sufficiently extensive. As such, the Adams et al. (2005) microseismic damage model is based  
74 on two critical assumptions, as follows:

- 75 1. the spatial extent of the ‘damage accumulation zone’ is sufficiently large and continuous  
76 that the low magnitude strains have sufficient opportunity to operate for a period of time  
77 sufficient to cause significant damage to rock. The exact spatial extent of the damage  
78 accumulation zone was not physically or theoretically constrained by Adams et al. (2005),  
79 but was suggested to be of the order of tens of metres inland from the cliff face. As such,  
80 ongoing microseismic strains were implicitly assumed to be able to cause damage at any  
81 location within the damage accumulation zone, to a degree commensurate with the  
82 magnitude of strain resulting from microseismic cliff flexure;
- 83 2. all microseismic ground displacements resulting from ocean wave loading of the  
84 foreshore platform create incremental rock-damaging strains. The magnitude of damage  
85 resulting from each load cycle was deemed to be a function of the magnitude of strain and  
86 the existing damage condition of the rock mass relative to its pristine state. Damage  
87 (weakening) was assumed to be cumulative and ongoing, increasing with the number of  
88 loading cycles experienced by the rock and, hence, through time.

89 We address these assumptions to provide an alternative interpretation of the potential  
90 effectiveness of microseismic ground motions in accumulating damage in rock and to  
91 reconsider the microseismic damage model proposed by Adams et al. (2005). We firstly  
92 present an alternative assessment of how and where microseismic ground motions are likely  
93 to act as an effective geomorphological process in brittle materials. Secondly, a 32-day record

94 of microseismic displacements recorded in a rocky coastal cliff environment is analysed to  
95 consider the key characteristics of the observed microseismic displacements to explore the  
96 possible temporal evolution of rock strength in response to microseismic loading. Thirdly, a  
97 conceptual model of the spatial and temporal occurrence of rock-damaging microseismic  
98 ground motions is developed. Finally, we explore the implications of the model and consider  
99 its potential validity using previously published datasets on rockfall activity in rocky coastal  
100 cliffs.

## 101 **2. Defining the damage accumulation zone**

### 102 2.1 Microseismic strain and stress magnitudes

103 Subcritical brittle microfracture and fatigue crack growth caused by cyclic loading have been  
104 shown to damage and weaken rocks in laboratory studies under compressive and tensile  
105 loading conditions (Attewell and Farmer, 1973; Lavrov et al., 2002; Erarslan and Williams,  
106 2012a). Such laboratory studies report results from tests that employ a variety of dynamic  
107 loading frequencies, including those comparable with the longer-period ground motions  
108 observed in coastal cliffs by Adams et al. (2005) and Young et al. (2011) (cf. Attewell and  
109 Farmer, 1973; Tien et al., 1990; Li et al., 1992). Attewell and Farmer (1973) concluded that  
110 the lowest frequencies tested (0.1 Hz; 10 s period) caused failure in fewer cycles than those  
111 of the same stress amplitude but higher frequency ( $\leq 20$  Hz; 0.05 s period), suggesting that  
112 ground motions resulting from foreshore wave loading, comparable to those observed by  
113 Adams et al. (2005) and Young et al. (2011) are potentially, in relative terms, highly  
114 damaging and conducive to fatigue crack growth.

115 Adams et al. (2005) and Young et al. (2012) estimated strains (dimensionless) resulting from  
116 microseismic ground motions of the order 0.1 to  $1 \times 10^{-6}$ . These estimated strain values are

117 many orders of magnitude lower than the peak strain values of rocks under monotonic  
118 loading (Young et al., 2012). For example, for a variety of rock types tested in unconfined  
119 compression, such peak strain values are in the range  $0.5 - 2 \times 10^{-2}$  (e.g. Heap et al., 2010).

120 Prior to failure, microseismic displacement and, hence, strain ( $\epsilon$ , i.e. relative displacement  
121 and deformation within the cliff-forming material) result in a (quasi-)proportional application  
122 of a stress ( $\sigma$ ) to the rock mass, following Hooke's law:

$$123 \quad \sigma = E\epsilon \quad (1)$$

124 where E is Young's modulus of elasticity. Applied microseismic stresses ( $\sigma_{\min}$  and  $\sigma_{\max}$ ) act  
125 relative to the mean (in situ static) stress ( $\sigma_{\text{mean}}$ ). Calculated and reported dynamic stresses  
126 resulting from microseismic loading are of the order 1 to  $10 \times 10^{-3}$  MPa (Adams et al., 2005;  
127 Young et al., 2012), assuming  $E = 20$  GPa. Peak unconfined compressive strength values  
128 (UCS) can range from 40 MPa (Bentheim Sandstone; Heap et al., 2009) to 360 MPa  
129 (Icelandic basalt; Vinciguerra et al., 2005). Rocks tend to be weaker under tensile loading  
130 conditions and peak tensile strength values can range from 4 MPa (Ellington Mudstone) to 70  
131 MPa (Cefn Coed Sandstone) (Hobbs, 1964). Stresses resulting from cliff flexure may  
132 therefore represent a greater proportion of peak (failure) stress under tensile baseline  
133 conditions.

## 134 2.2 Brittle microfracture and subcritical crack growth

135 Whilst stresses and strains induced by microseismic ground motions are a small fraction of  
136 peak values observed under monotonic loading, localised brittle microfracture damage can  
137 occur in rock at stresses significantly less than peak strength (Scholz, 1968; Martin and  
138 Chandler, 1994; Mitchell and Faulkner, 2008). The macro-scale mechanical behaviour of

139 rock in the brittle domain is dependent on rock microstructure (Potyondy, 2007), notably the  
140 presence, density and interaction of microcracks (Tapponier and Brace, 1976; Eberhardt et  
141 al., 1999). The remotely applied microseismic stresses are not necessarily transmitted equally  
142 throughout the rock mass (Potyondy, 2007). Stress magnitudes can be locally modified within  
143 the rock mass at sites of stress concentration, such as pore spaces, grain or crystal boundaries,  
144 microscopic flaws and petrological structures (Cai et al., 2004), allowing microcrack  
145 nucleation as stresses exceed local strength (Kranz, 1983). The magnitude of the elastic stress  
146 field at the microcrack tip is described by  $K$ , the stress intensity factor (cf. Janssen et al.,  
147 2002, for example), defined as:

$$148 \quad K = \sigma\sqrt{\pi a} \quad (2)$$

149 where  $\sigma$  is the remotely applied stress and  $a$  is the microcrack length. Equation (2) describes a  
150 an isolated two-dimensional crack in an infinite space, which we use for simplicity but note  
151 that alternative terms are required for microcracks of differing geometry (cf. Brady and  
152 Brown, 2004). Increasing  $K$  values results in an increase in the potential for microcrack  
153 growth (Janssen et al., 2002).

154 When populations of microcracks are sufficiently dense to permit interaction at a critical  
155 scale, crack coalescence results, ultimately culminating in macro-scale fracture (Bieniawski,  
156 1967; Martin and Chandler, 1994; Main et al., 1993). The process of microcrack propagation  
157 and coalescence can result in measurable and continuous pre-failure macro-scale strains that  
158 culminate in slope failure or rockfall activity at the field scale (Petley et al., 2005a, b; Rosser  
159 et al., 2007; Stock et al., 2011).

### 160 2.3 Damage thresholds and cyclic stress amplitudes

161 There are key differences between laboratory dynamic loading tests and microseismic  
162 loading conditions experienced and observed in the field. The stress amplitudes reproduced in  
163 strain-controlled tests under laboratory conditions are significantly greater than those that  
164 result from microseismic displacements observed by Adams et al. (2005) and Young et al.  
165 (2011; 2012). For example, the cyclic stress amplitude range used by Attewell and Farmer  
166 (1973) increased the maximum dynamic compressive stress to between 40 and 75 % of the  
167 UCS (57 to 130 MPa) of the dolomite samples used; mean compressive stresses were  
168 between 25 % and 50 % of the UCS. Similarly, dynamic stresses applied to Belgian ‘blue’  
169 limestone by Lavrov et al. (2002) were between 50 and 70 % of the peak Brazilian tensile  
170 strength observed. These high stress amplitudes employed in dynamic laboratory tests were  
171 sufficient to nucleate microcracks. The level of stress required to initiate microcracking is  
172 described by the staged brittle failure model conceptualised and developed by Brace et al.  
173 (1966), Bieniawski (1967) and Martin and Chandler (1994) (Fig. 1 a), which we use as a  
174 conceptual basis on the assumption that similar thresholds are observed under tensile and  
175 shear loading conditions (see Lavrov et al., 2002; Jafari et al., 2003). In a typical strain-  
176 controlled monotonic compression test, the microcracking process is characterised by five  
177 key stages:

- 178 1. Crack closure, as pre-existing and microcracks favourably oriented to the applied load  
179 close. The stress-strain curve is non-linear, displaying an increase in stiffness;
- 180 2. Linear elastic deformation, which occurs when the majority of microcracks have closed at  
181  $\sigma_{cc}$ , the crack closure stress threshold;
- 182 3. Crack initiation and stable crack growth occur as the stress level for crack initiation,  $\sigma_{ci}$ , is  
183 exceeded.  $\sigma_{ci}$  occurs at approximately 30 – 50 % of the peak strength,  $\sigma_{fs}$  (Brace et al.,  
184 1966; Eberhardt et al, 1999). Microcracks grow in the direction of the major principal

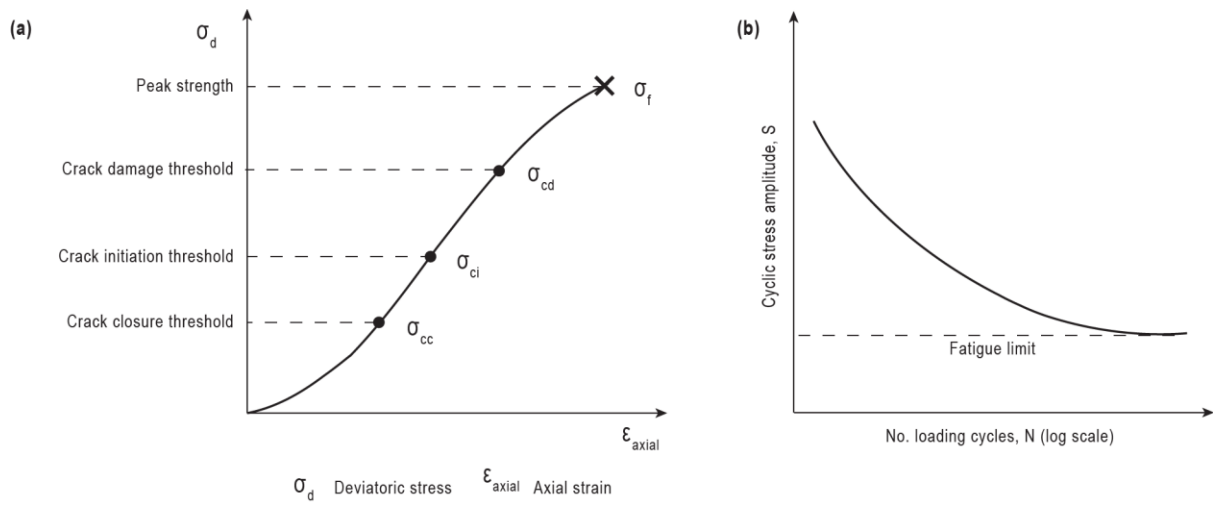


185 stress,  $\sigma_1$  (Hoek and Bieniawski, 1965; Lajtai, 1971; Peng and Johnson, 1972). In the  
186 stable crack growth stage under monotonic loading, removal of the applied load can stop  
187 crack growth, or limit the rate of growth (Eberhardt et al., 1999);

188 4. Crack damage and unstable crack growth occur as stress levels exceed the crack damage  
189 threshold,  $\sigma_{cd}$ . This point may be evident as a clear reduction in stiffness on the stress-  
190 strain curve (Fig. 1 a) and results from microcrack coalescence and an accelerating crack  
191 growth rate that cannot be halted by removing the applied stress (Bieniawski, 1967).  $\sigma_{cd}$   
192 occurs between 70 and 90 % of  $\sigma_{fs}$  (Bieniawski, 1967); and

193 5. Failure at  $\sigma_f$  followed by post peak behaviour, which in fully fractured brittle materials  
194 may not be present.

195 Eberhardt et al. (1999) demonstrated that characteristic normalised axial strains exist for each  
196 of the microcracking thresholds under compressive loading conditions. Crack initiation  
197 occurs at approximately 45 % of the peak strain at failure and crack damage and propagation  
198 occurs at strains greater than approximately 68 % of the peak failure strain (Eberhardt et al.,  
199 1999).



200

201 Fig. 1. (a) Stress-strain curve showing the stages of crack development (adapted from  
 202 Eberhardt et al., 1999) (b) Typical S-N curve for materials showing a fatigue limit.

203 Critical stress and strain levels have previously been emphasised in field and modelling  
204 studies. Exceedance of the crack initiation threshold,  $\sigma_{ci}$ , creates a sufficiently dense  
205 population of microcracks that can subsequently be exploited by ‘environmental’ forces  
206 (Rosser et al., 2007), such as variations in pore water pressure (Petley et al., 2005a, b; Ng and  
207 Petley, 2009), ambient temperature (Gischig et al., 2011a, b) and/or potentially ocean wave  
208 impact loads (Adams et al., 2002). These processes cause further accumulation of damage  
209 resulting from, for example, time-dependent creep and fatigue processes driven by subcritical  
210 crack growth (Rosser et al., 2007). In turn, this can cause stress redistribution and further  
211 microcrack damage in a progressive failure process (Terzaghi, 1962; Bjerrum, 1967;  
212 Eberhardt et al., 2004), causing the crack damage threshold,  $\sigma_{cd}$ , to be exceeded, triggering a  
213 transition from secondary to tertiary creep and, ultimately, rupture (Petley et al., 2005a, b).

214 Importantly, critical stress and strain levels are required to nucleate microcracks before  
215 fatigue processes can exert an influence on microcrack densities and rock strength. Such  
216 critical stressing is achieved in the high cyclic stress amplitude laboratory tests undertaken by  
217 Attewell and Farmer (1973), for example. However, where  $\sigma_{mean}$  does not exceed  $\sigma_{ci}$ , small  
218 fluctuations in the stress field generated by microseismic ground displacements are highly  
219 unlikely to be of sufficient magnitude to increase the stress state to a level that can induce  
220 crack initiation and unstable crack growth.

221 The importance of stress amplitude in causing failure in materials subjected to dynamic  
222 loading can also be demonstrated by plotting stress amplitude,  $S$ , against number of cycles to  
223 failure,  $N$  (logarithmic scale), to produce S-N curves (Fig. 1 b). Each point used to define the  
224 curve reflects a single specimen that has been subjected to constant amplitude loading until  
225 failure. Critically, however, not all stress amplitudes result in failure, as demonstrated by the

226 plateau in the S-N curve. There is a threshold stress amplitude, the fatigue limit ( $\sigma_f$ ). Cyclic  
227 stress amplitudes less than  $\sigma_f$  do not result in growth of fatigue cracks and, hence, rocks can  
228 be subjected to an infinite number of stress cycles at this stress amplitude (Janssen et al.,  
229 2002). Full characterisation of fatigue strength requires S-N curves to be obtained for all  
230 mean stress conditions and for compressive, tensile and shear stresses (cf. Attewell and  
231 Farmer, 1973; Jafari et al., 2003; Lavrov et al., 2002; Erarslan and Williams, 2012a). Greater  
232 mean stress values result in a decreasing resistance to smaller amplitude loads (Suresh, 1998).  
233 This effect is likely to be significant when mean deviatoric stress is greater than the  $\sigma_{ci}$ ,  
234 resulting in a microfracture population that is prone to fatigue crack growth during cyclic  
235 loading (Attewell and Farmer, 1973).

#### 236 2.4 Loading direction

237 The existence of the crack closure stage in the microcrack development model described  
238 above suggests that the direction of stress application relative to pre-existing flaws may be  
239 important during cyclic loading, particularly in rocks displaying marked micro-structural  
240 anisotropy (e.g. Nasser et al., 2010). However, the directional component of microseismic  
241 cyclic loading is currently poorly constrained and the effects of variability in loading  
242 direction are not explicitly considered in the microseismic damage model of Adams et al.  
243 (2005).

#### 244 2.5 Fatigue damage accumulation zones

245 The discussion presented above suggests that microseismic ground motions require intact  
246 rocks to have experienced a critical level of stress and strain (i.e. a pre-damaged condition)  
247 before they can propagate microfractures and accelerate their growth. Critical stressing  
248 reduces the value of the fatigue limit,  $\sigma_f$ , allowing low cyclic stress amplitudes generated by

249 microseismic ground motions to cause fatigue crack growth. In order to define the nature of  
250 fatigue damage accumulation zones, it is necessary to consider where such critical stressing  
251 occurs in geomorphic systems. We can speculate with reasonable confidence on the basis of  
252 published results and theory, but it is emphasised that we cannot yet exactly define the level  
253 of critical stressing and the associated value (or range of values) of  $\sigma_f$  required to permit the  
254 microseismic stresses generated in a geomorphic setting to be effective in causing fatigue.

255 In the context of a coastal rock cliff, or indeed any rock slope, stress distributions are  
256 controlled by cliff height and local (near-cliff face) stress concentrations that result from  
257 slope angle, cliff face geometry and the presence and nature of asperities at a variety of  
258 spatial scales (Jafari et al., 2003; Wolters and Müller, 2008; Young and Ashford, 2008;  
259 Wyllie and Mah, 2010; Gischig et al., 2011a, b; Stock et al., 2011; Styles et al., 2011).  
260 Modelling work by Wolters and Müller (2008) suggested that shear stresses along (potential)  
261 slip surfaces reduce significantly in the first few metres from the cliff face, suggesting that  
262 the critical stressing necessary to form microcracks and, hence, increase susceptibility to  
263 cyclic damage processes is more likely to have been achieved close to the cliff face and so  
264 microseismic fatigue may be more effective here. Styles et al. (2011) demonstrated how  
265 critical levels of stress propagate along a spatially concentrated failure surface that is  
266 relatively close to the cliff face ( $10^0$  to  $10^1$  m). In both of these modelling studies, deviatoric  
267 stress and resultant strain are shown to quickly reduce to lower levels with perpendicular  
268 distance from the fracture surface. The same distance-decay effect in stress and damage away  
269 from the fracture surface has previously been reported in major tectonic fault zones (Anders  
270 and Wiltschko, 1994; Moore and Lockner, 1995; Vermilye and Scholz, 1998; Janssen et al.,  
271 2001; Wilson et al., 2003; Faulkner et al., 2006). Such observed exponential decreases in

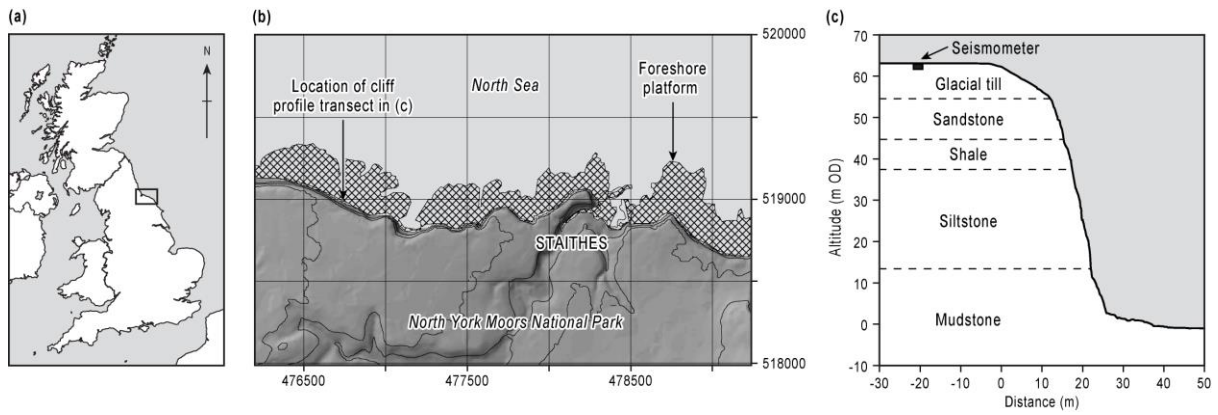
272 microcrack density have been interpreted to reflect the stress gradient away from the fracture  
273 (fault) (Mitchell and Faulkner, 2008).

274 A strong spatial pattern in the effectiveness of microseismic ground motions in propagating  
275 and connecting microcrack populations results from this spatial pattern of in situ stresses. The  
276 critical levels of stress and strain (i.e. exceedance of the crack initiation threshold as a  
277 minimum) required to reduce the fatigue limit to a level that can be exploited by  
278 microseismic ground displacements only occur in spatially restricted circumstances. Rock  
279 that is not within a critically-stressed fatigue damage accumulation zone surrounding pre-  
280 formed and incipient fractures may therefore be considered unlikely to undergo microseismic  
281 fatigue damage.

### 282 **3. Magnitude and frequency of rock-damaging microseismic ground displacements**

#### 283 3.1 Study site

284 The study site is a section of the coastline on the North York Moors National Park in  
285 northeast England located approximately 1.5 km to the east of the village of Staithes (Fig. 2).  
286 This section of coastline has been previously been studied by Agar (1960), Robinson (1974),  
287 Lim et al. (2010; 2011), Rosser et al. (2007), Barlow et al. (2012), Norman (2012) and  
288 Norman et al. (in revision), providing a baseline dataset on cliff erosion rates, patterns of  
289 rockfall activity and energy delivery to coastal cliffs.



290

291 Fig. 2. (a) Map of the United Kingdom showing the approximate location of the North  
 292 Yorkshire coastline (boxed area). (b) Study site location on the coast of the North York  
 293 Moors National Park. Hatched area denotes the foreshore platform. 25 m topographic  
 294 contours are from Ordnance Survey PlanForm data (under license from EDINA, 2010). (c)  
 295 Cross-section of the coastal cliff study site at Boulby obtained using Terrestrial Laser  
 296 Scanning (see Rosser et al., 2007 and references therein) displaying seismometer installation  
 297 location and schematic display of cliff lithology.

298 The cliffs at our study site are oriented approximately  $290^\circ$  to c.  $110^\circ$ , generating exposure to  
299 easterly and northerly North Sea storm events, but shelter from prevailing southwesterly  
300 weather systems.

301 The c. 70 m high, near-vertical cliffs at the site are cut into the interbedded mudstones,  
302 shales, siltstones, ironstones and sandstones of the Lower Jurassic Redcar Mudstone and  
303 Staithes Sandstone formations (Rawson and Wright, 2000), which dip at  $2^\circ$  to the southeast  
304 and are capped by approximately 10 m of overconsolidated Devensian glacial till.

305 The site has a tidal range of c. 6 m. This submerges the base of the cliff (approximately 1.6  
306 m above Ordnance Datum – approximately mean sea level) during high spring tides. The  
307 cliffs are fringed by a foreshore platform that extends approximately  $> 200$  m seaward (Fig.  
308 2) and is fully exposed when high atmospheric pressure systems coincide with lowest  
309 astronomical tides. Beach deposits are generally absent. Wave fetch at the site is limited in  
310 most directions by the boundary coasts of the North Sea. In turn, this controls and limits the  
311 wave periods that can develop. The Cefas WaveNet wave buoy located approximately  $\sim 18$   
312 km to the northwest of the site recorded a mean wave period of approximately 5 s and a  
313 model value of 3 – 4 s between July 2008 and July 2010 (Norman, 2012).

## 314 3.2 Methods

### 315 3.2.1 Microseismic data

316 Ground motions were measured using a Gralp 6TD broadband seismometer, which has a flat  
317 frequency response range 0.033 to 100 Hz (period response range of 30 to 0.01 s). We  
318 monitored velocity (m/s) in three axes (vertical, z; north-south, n; and east-west, e) at a  
319 sampling rate of 100 Hz (Nyquist frequency of 50 Hz). The seismometer location is displayed  
320 in Fig. 2. Further details on seismometer installation, data collection and quality screening to



321 check for and remove any anthropogenic noise or earthquakes signals are provided by  
322 Norman (2012) and Norman et al. (in revision). Notably, a considerable section of  
323 microseismic data that is ostensibly not related to the local and/or regional signals of  
324 interested here has been removed from 15 July 2009 (Fig. 3 a).

325 Ground tilt causes a component of the vertical gravitational acceleration to be recorded in the  
326 horizontal acceleration channels (Rodgers, 1968). Whilst tilt ‘contamination’ of the vertical  
327 component is generally considered minimal (Graizer, 2006), recorded horizontal (e and n)  
328 acceleration (and hence velocity and displacement) can be overestimated unless corrected for  
329 (Young et al., 2012). The effects of ground tilt on horizontal displacement increase with  
330 increasing period (Webb and Crawford, 1999; Crawford and Webb, 2000) but have been  
331 shown to be minimal at frequencies less than 0.14 Hz (~7 s period) (Young et al., 2012). To  
332 avoid the effects of tilt on our displacement data, we consider the frequency band 0.14 – 1 Hz  
333 (1 – 7 s period). In addition, we refer to horizontal (e and n) displacements as ‘apparent’ to  
334 signify that no tilt corrections have been applied. To obtain the selected frequency band, we  
335 applied a bandpass filter to the output velocity data for each component of ground motion (z,  
336 n and e). We subsequently integrated the filtered velocity data with trapezoidal accuracy to  
337 obtain time-series of displacement data ( $\mu\text{m}$ ), which retain the same sampling frequency (100  
338 Hz) of the original velocity data.

339 As described above, the 1 – 7 s period band contains both the mean and model wave periods  
340 recorded offshore. Norman et al. (in revision) demonstrated a landward decay in the vertical  
341 energy signal recorded at additional seismometers placed in a cross-shore transect for 1, 2  
342 and 5 s period ground motions at the site. Since the microseismic signals recorded are not  
343 uniform at all seismometers, such signals are deemed to be above background levels. In

344 addition, the cross-shore decay in energy signal suggests a similar cliff flexure and strain  
345 signal that results from foreshore loading by incident swell waves, as observed at other sites  
346 (cf. Adams et al., 2005; Young et al., 2011; 2012). Hence, the 1 – 7 s period band is  
347 appropriate for our study on the assumption that the displacements recorded at our  
348 seismometer are observed at greater magnitude closer to the cliff edge and decay in  
349 magnitude with distance inland.

350 Results are presented from two 16-day periods: 2 to 17 July 2009; and 27 November to 12  
351 December 2009. These were selected to represent typical ‘summer’ and ‘winter’ conditions  
352 on the North Yorkshire coastline.

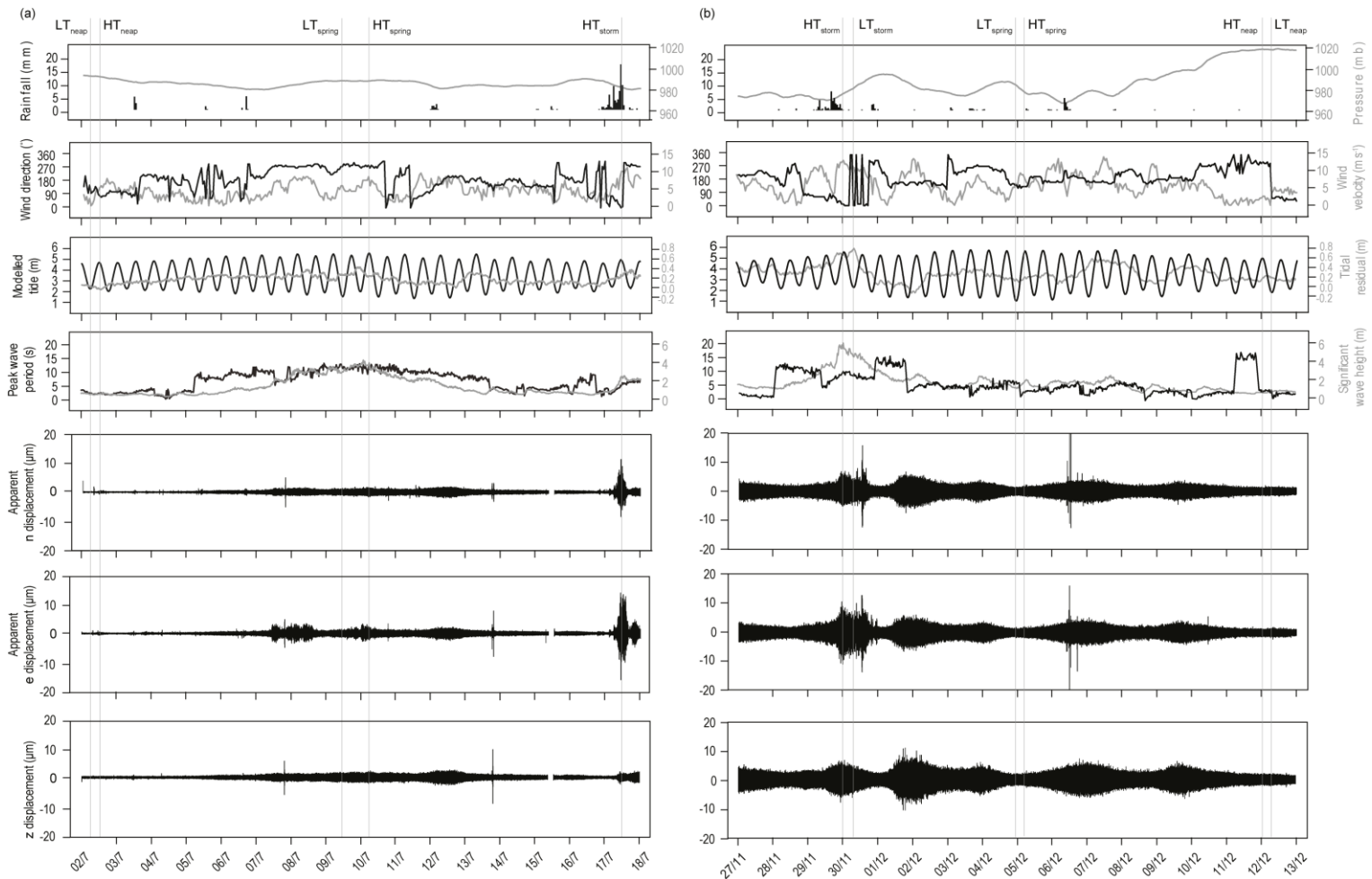
### 353 3.2.2 Meteorological, hydrographic and oceanographic data

354 Prevailing weather data (rainfall, atmospheric pressure, wind direction and wind velocity),  
355 collected at five-minute intervals, were obtained from the UK Meteorological Office  
356 monitoring station Loftus, 1.5 km west of the site.

357 Tidal (predicted tidal height and observed tidal residual) data were obtained for Whitby,  
358 approximately 15 km to the southeast of Staithes, from the British Oceanographic Data  
359 Centre, and oceanographic (significant wave height and peak wave period) from a wave buoy  
360 ~18 km offshore. Time series plots of meteorological, tidal, oceanographic and microseismic  
361 displacement data for the July 2009 and November/December 2009 monitoring periods are  
362 displayed in Fig. 3 (a and b, respectively).

363 These datasets are used to consider general ‘environmental’ conditions in the region and,  
364 hence, at our study site. We do not consider the modifying effects of nearshore bathymetry on

365 oceanographic and hydrographic conditions here; further analysis of such effects is provided  
366 in Norman et al. (in revision).



367

368 Fig. 3. Time series plots of meteorological, tidal, oceanographic and microseismic data for (a) July 2009 monitoring period and (b) November-  
 369 December 2009 monitoring period. Vertical grey lines indicate the centre-point of characteristic displacement scenarios discussed in the text.  
 370 Black datasets correspond to left-hand vertical axes. Grey datasets correspond to right-hand vertical axes. Gap in seismic data on 15 July 2009  
 371 reflects manual removal of ground motions not explained by local conditions, in accordance with Adams et al. (2005) and Young et al. (2012).  
 372 See main text for an explanation of notation.

### 373 3.3 Microseismic data

#### 374 3.3.1 General patterns and controls on displacement magnitude

375 Cliff ground motion responds to both proximal and distal loading, and can be broadly  
376 correlated with marine and weather conditions (Norman, 2012; Norman et al., in revision). In  
377 both July 2009 (Fig. 3 a), microseismic ground displacements generally exhibit low  
378 amplitudes that range from approximately  $-1\ \mu\text{m}$  to  $1\ \mu\text{m}$  in z, n and e directions, punctuated  
379 by periods of greater displacement. In November/December 2009, 'background'  
380 displacements are marginally greater, ranging from  $-2\ \mu\text{m}$  to  $2\ \mu\text{m}$ , but a similar pattern of  
381 periods of elevated displacements can be seen.

382 On 17 July 2009, a prolonged period of elevated microseismic activity was observed, with  
383 peak displacement amplitudes reaching maxima of  $\sim 12\ \mu\text{m}$  and  $\sim 16\ \mu\text{m}$  in the n and e  
384 directions respectively, though elevated ground displacements above 'background' levels in  
385 the z direction are less pronounced. In November/December 2009, a similar prolonged and  
386 high amplitude episode of displacement occurred between 29 and 30 November. Again, this  
387 is mostly apparent in the n and e directions, which displayed peak amplitudes of  $\sim 10\ \mu\text{m}$  but  
388 also shorter-lived peak displacements of  $\sim 15\ \mu\text{m}$ . Further elevated, yet less sustained, ground  
389 displacements occurred on 6 December 2009.

390 A thorough analysis of environmental controls on microseismic displacement is beyond the  
391 scope of this paper (see Norman, 2012; and Norman et al., in revision). However, qualitative  
392 comparison of environmental and microseismic datasets (Fig. 3) suggests that the majority of  
393 the elevated amplitude ground displacements results from a critical combination of key  
394 prevailing meteorological, tidal and oceanographic conditions that are typical of infrequent  
395 storm events. These events are characterised by reduced atmospheric pressure, increased

396 rainfall, high velocity onshore winds, high tidal residuals and elevated significant wave  
397 heights (Fig. 3).

### 398 3.3.2 Characteristic displacement scenarios

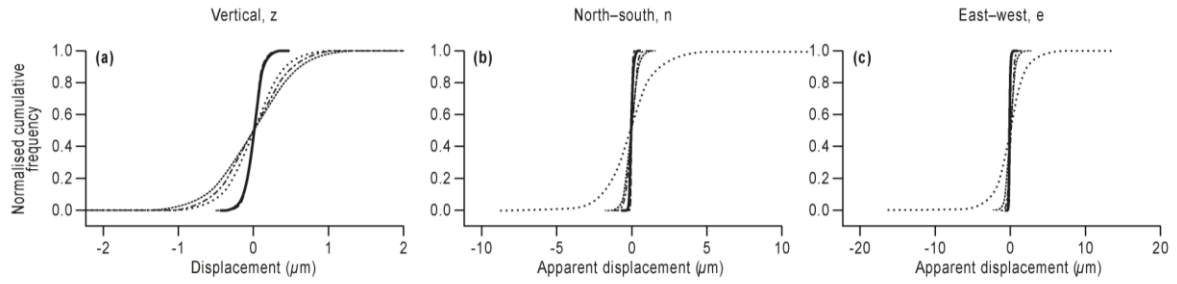
399 To consider variations in microseismic displacement more fully, periods during which  
400 particular environmental conditions prevail (i.e. ‘displacement scenarios’) are now examined.  
401 For both datasets (July and November/December 2009) we consider examples of  
402 displacement during both low and high tide conditions during a neap tidal phase ( $LT_{neap}$  and  
403  $HT_{neap}$  respectively), and during low and high tide conditions during a spring tidal phase  
404 ( $LT_{spring}$  and  $HT_{spring}$  respectively). In addition the effects of storm conditions during the  
405 November/December 2009 period are examined (Fig. 3 b) during both low and high tide  
406 conditions ( $LT_{storm}$  and  $HT_{storm}$  respectively), and in July 2009 (Fig. 3 a) during high tide  
407 conditions ( $HT_{storm}$ ). Given the semidiurnal tidal cycle, we define the duration of each  
408 displacement scenario as a three-hour time window (i.e.  $1.08 \times 10^6$  observations) centred on  
409 the tidal maxima (high tide) or minima (low tide). These time periods selected are shown in  
410 Fig. 3.

### 411 3.3.3 Displacement magnitude

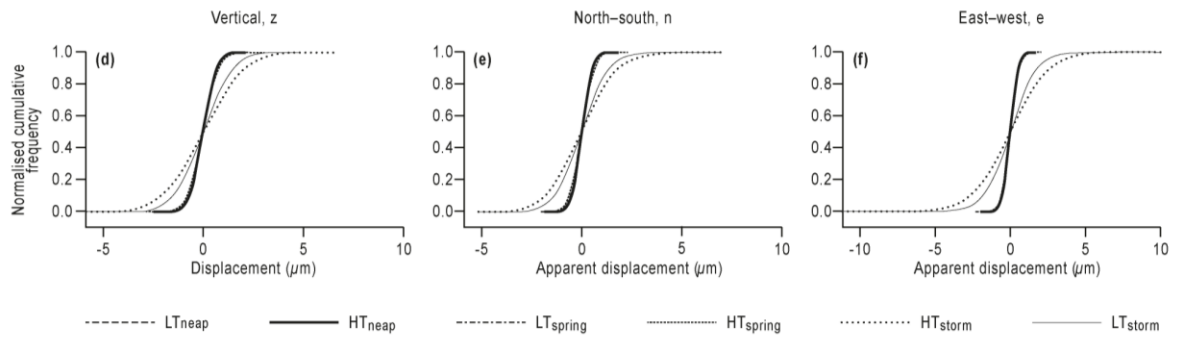
412 Since displacement and strain are related to stress change (Equation 1), we firstly  
413 demonstrate the relative frequency of displacements across the full spectrum of observed  
414 displacement magnitudes during each characteristic scenario. Normalised cumulative  
415 frequency plots of displacement for each scenario and for each component of ground motion  
416 (z, n and e) are displayed in Fig. 4.

417

July 2009



November/December 2009



418

419 Fig. 4. Normalised cumulative frequency plots of displacement for July 2009 (a – c) and  
420 November-December 2009 (d – f). See main text for an explanation of notation.

421 Tidal control on displacement amplitude is apparent but is less pronounced than in previously  
422 published studies (cf. Adams et al., 2005). In July 2009, the standard deviation of  
423 displacement ranges from  $\sim 0.1 \mu\text{m}$  (neap tides) to  $\sim 0.5 \mu\text{m}$  (spring tides) in the z, n and e  
424 components. The maximum peak displacement amplitudes observed during neap and spring  
425 conditions in the absence of storm events are  $\sim 0.3 - 3.0 \mu\text{m}$ . In November/December 2009,  
426 the standard deviation of displacement ranges from  $\sim 0.4 \mu\text{m}$  (neap tides) to  $\sim 0.6 \mu\text{m}$  (spring  
427 tides) in the z, n and e components. The maximum peak displacements amplitudes observed  
428 range from  $\sim 1.5 - 3.0 \mu\text{m}$  in the z, n and e components.

429 The control of storm events in generating greater displacement amplitudes is apparent in both  
430 the n and e components during both high and low tide conditions. During  $HT_{\text{storm}}$  in both July  
431 2009 and November 2009, standard deviations of peak displacement amplitude reached  $\sim 2$   
432  $\mu\text{m}$  in both the n and e components. Some tidal control on displacement during storms is  
433 apparent in November 2009; standard deviations of displacement amplitude are lower during  
434  $LT_{\text{storm}}$  (n component:  $1.1 \mu\text{m}$ ; e component:  $1.5 \mu\text{m}$ ) than during  $HT_{\text{storm}}$  conditions (n  
435 component:  $1.5 \mu\text{m}$ ; e component:  $2.1 \mu\text{m}$ ).

436 Very infrequently occurring ( $p < 0.0001$ ) peak displacement amplitudes observed during  
437 'storm' conditions are an order of magnitude greater than those observed under non-storm  
438 conditions, reaching  $\sim 16 \mu\text{m}$  in the e component in July 2009 ( $HT_{\text{storm}}$ ) and  $\sim 11 \mu\text{m}$  in the e  
439 component in November 2009. The effect of storm events on displacement in the z direction  
440 is less pronounced within the frequency band considered.

#### 441 3.3.4 Displacement direction

442 Since the direction of displacement and, hence, stress application may be of significance for  
443 fatigue crack growth (Section 2.4), it is important to consider the directional component of



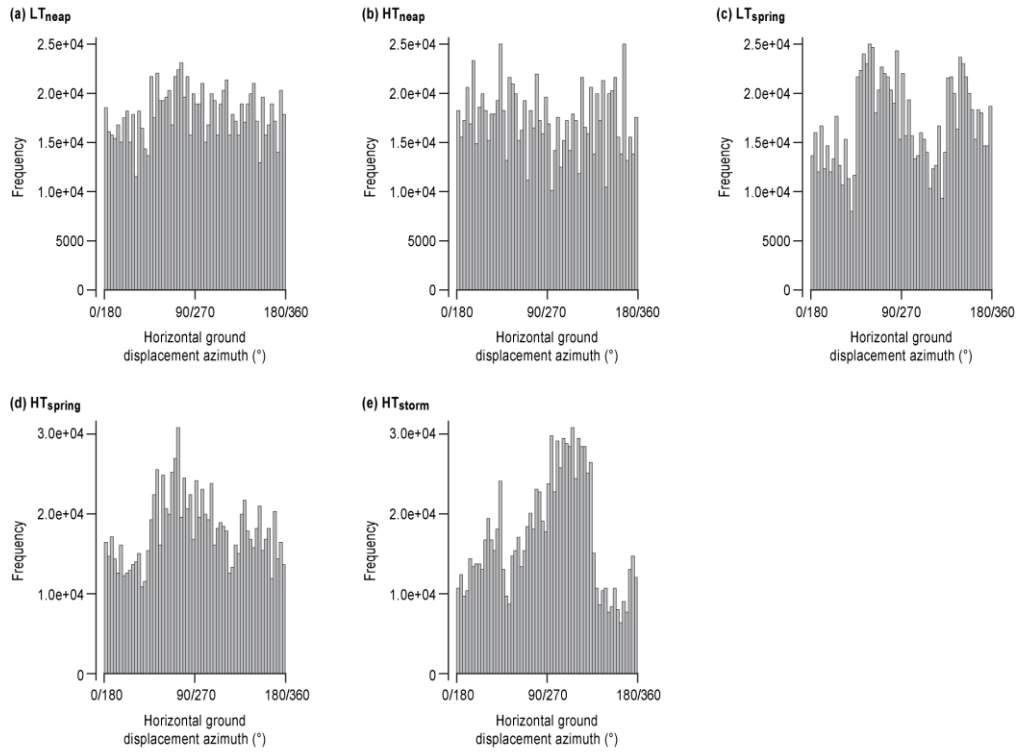
444 microseismic motion for each of the displacement scenarios. For exemplary purposes, we  
445 consider the horizontal component of ground motion only. Principal Component Analysis  
446 was undertaken on successive groups of 350 observations (i.e. 3.5 s of data per group, a  
447 duration equal to the modal wave period observed offshore; Section 3.1). For each 3.5 s  
448 group, the resultant azimuth of horizontal ground motion was calculated. Histograms of the  
449 frequency distribution of the azimuth of horizontal ground motion for each characteristic  
450 displacement scenario are given in Fig. 5.

451 In July 2009, horizontal ground displacements displayed little, if any, preferential direction  
452 during  $LT_{\text{neap}}$  and  $HT_{\text{neap}}$  (Fig. 5). During  $LT_{\text{spring}}$  and  $HT_{\text{spring}}$ , ground displacement frequency  
453 distributions display bimodality, with peaks at c.  $60^\circ/240^\circ$  and  $150^\circ/330^\circ$ , though the latter is  
454 less pronounced for  $HT_{\text{spring}}$ . During  $HT_{\text{storm}}$  for July 2009, modal peaks in ground  
455 displacement frequency exist at  $45^\circ/225^\circ$  and, most clearly, at  $110^\circ/290^\circ$ , which is  
456 approximately cliff-parallel. The least frequently observed horizontal ground displacement  
457 azimuths occurred between  $135^\circ/315^\circ$  and  $165^\circ/345^\circ$  during  $HT_{\text{storm}}$  (Fig. 5).

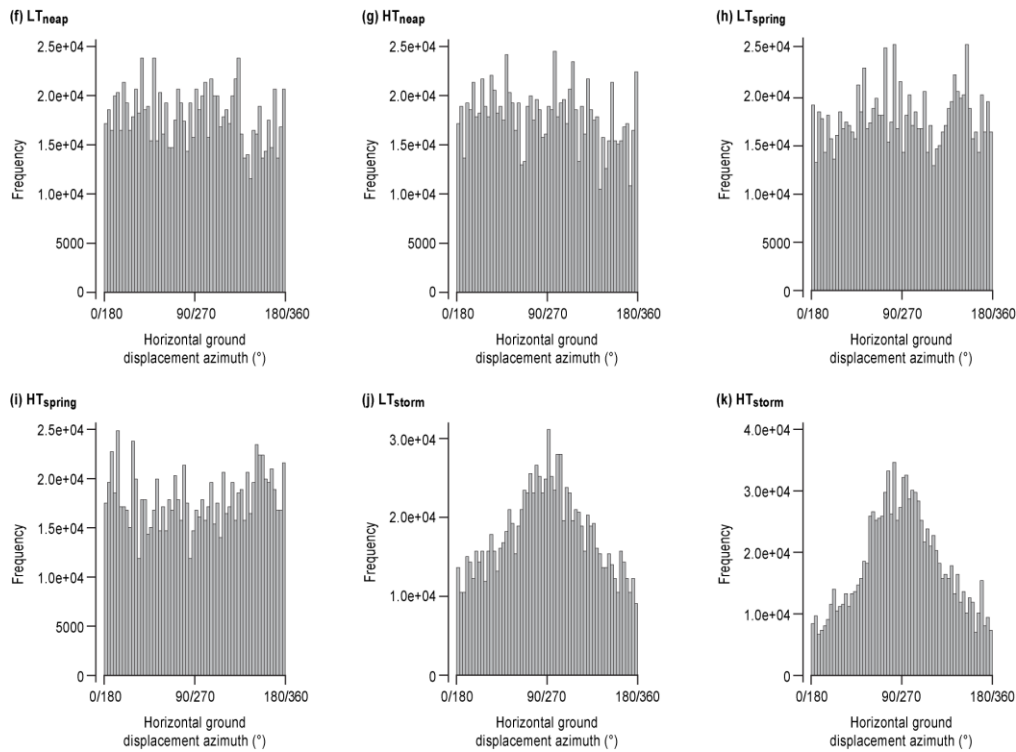
458 Horizontal ground displacements in November/December 2009 also displayed limited  
459 obvious preferential motion azimuths during  $LT_{\text{neap}}$ ,  $HT_{\text{neap}}$ ,  $LT_{\text{neap}}$  and  $HT_{\text{neap}}$ . In contrast,  
460 during  $LT_{\text{storm}}$  and  $HT_{\text{storm}}$ , a clear modal peak in ground displacement azimuth exists at  
461  $\sim 90^\circ/270^\circ$ , which again is approximately cliff-parallel (Fig. 5). The least frequently observed  
462 horizontal ground displacement azimuths occurred broadly in the north-south direction  
463 (approximately cliff-normal) during  $LT_{\text{storm}}$  and  $HT_{\text{storm}}$  (Fig. 5).

464

July 2009



November/December 2009



465

466 Fig. 5. Frequency distributions of azimuth of horizontal ground displacement for  
467 characteristic displacement scenarios for July 2009 (a to e) November-December 2009 (f to  
468 k). See main text for an explanation of notation.  
469

470 Implications

### 471 3.3.5 Variable stress amplitude loading

472 Our data suggest that coastal rock cliffs are subjected to varying cyclic stress amplitudes.  
473 Since conventional S-N curves are developed using constant amplitude loading, they are not  
474 appropriate in assessing rates of damage accumulation in this setting. Conventional fracture  
475 mechanics suggests that varying microseismic displacement amplitudes will profoundly  
476 affect the rate of fatigue-driven crack growth following crack initiation, and only if dynamic  
477 stress amplitudes are sufficient. The greater cyclic stress amplitudes that occur during storm  
478 events will result in a greater change in the crack tip intensity,  $K$  (Equation 2). This opens the  
479 crack beyond that resulting from background cyclic loads, but also creates a large plastic  
480 damage zone around the crack tip (Faulkner et al., 2011), and potentially blunting the crack  
481 tip (Suresh, 1998; Petley and Petley, 2006). This results in a localised stress drop as local  
482 peak strength is exceeded (cf. Mitchell and Faulkner, 2008) and a less severe stress  
483 concentration than that at a sharp crack tip (Suresh, 1998).

484 During non-storm conditions, the more frequent lower amplitude cyclic stresses may cause  
485 the microcrack to grow into the plastic zone created during ‘storm’ loading, resulting in a  
486 short-lived increase in the rate of microcrack growth. However, high residual compressive  
487 stresses now exist within the plastic zone due to the surrounding elastically stressed material  
488 that is yet to fail (Janssen et al., 2002). Residual deformation is created in the areas  
489 previously occupied by the crack tip plastic zone, causing microcrack closure (Janssen et al.,  
490 2002). Together, these effects may in theory result in a significantly reduced rate, or indeed a  
491 cessation, of crack growth that persists until the microseismic stress is increased to a level  
492 that is greater than that previously experienced (cf. Lavrov, 2005; Petley et al., 2005 a, b).

493 This ‘additive’ and dynamic threshold is key to defining the location and timing of when  
494 microseismic ground motions can be effective.

### 495 3.3.6 Variability in loading direction

496 The most frequently experienced microseismic loading conditions display a characteristic and  
497 limited range of loading directions, with no sustained preferential loading direction. The  
498 result is likely to be a constrained stress distribution and plastic zone at the crack tip.  
499 Consequently, the rate of crack growth is controlled by the magnitude, frequency and  
500 sequencing of displacements, and any resultant thresholds, as defined above. When rare  
501 displacement directions, such as those with a greater cliff normal (north-south) component in  
502 our study, are experienced, a change to the microscale (crack tip) stress field may result. This  
503 may cause greater damage to the rock as the change in loading direction may alter the crack  
504 tip separation mode. For example, a Mode I (extension/opening) crack may, under less  
505 frequent microseismic loading directions, experience sufficiently significant Mode II (in-  
506 plane shear) or Mode III (out-of-plane shear) deformation (Paterson, 1978). Microcracks may  
507 as a result switch failure mode or become mixed-mode (Brady and Brown, 2004), promoting  
508 growth into previously intact rock, the interaction of otherwise-isolated microcrack  
509 populations (cf. Lavrov et al., 2002), and ultimately an increased microcrack density, rock  
510 dilatancy and damage (Eberhardt et al., 1999). Changes in loading direction may exploit  
511 lithological and structural anisotropy, such as the presence of bedding planes and pre-existing  
512 fracture sets that display greater sensitivity to favourably-oriented stress perturbations (cf.  
513 Suresh, 1998). The effects of structural anisotropy and variable microscopic failure  
514 mechanics are apparent at the both the laboratory (McLamore and Gray, 1967; Niandou et al.,

515 1997; Erarslan and Williams, 2012b) and field scale (Giraud et al., 1990; Agliardi et al.,  
516 2001).

### 517 3.3.7 Episodic damage

518 We surmise that microcrack-driven weakening as a result of microseismic ground  
519 displacements may be an highly episodic process. We suggest that microseismic conditions  
520 conducive to microcrack propagation, rock damage and a reduction in in peak strength values  
521 are only likely to occur extremely rarely, though the frequency of such rare conditions  
522 remains difficult to quantify, particularly on the basis of relatively short observational  
523 records. These favourable conditions are likely to occur during energetic storm events that  
524 infrequently punctuate the lower amplitude microseismic displacements that result from the  
525 cyclic ocean wave loading of the foreshore platform. During energetic events (storms),  
526 sufficiently high stresses are only generated for a very small fraction of their duration, and  
527 indeed are only effective if the previous maximum dynamic stress damage threshold is  
528 exceeded. This threshold also depends on the coincidence of two infrequent and apparently  
529 independent occurrences: high magnitude displacements (strains) and a rarely-occurring  
530 microseismic loading direction (azimuth).

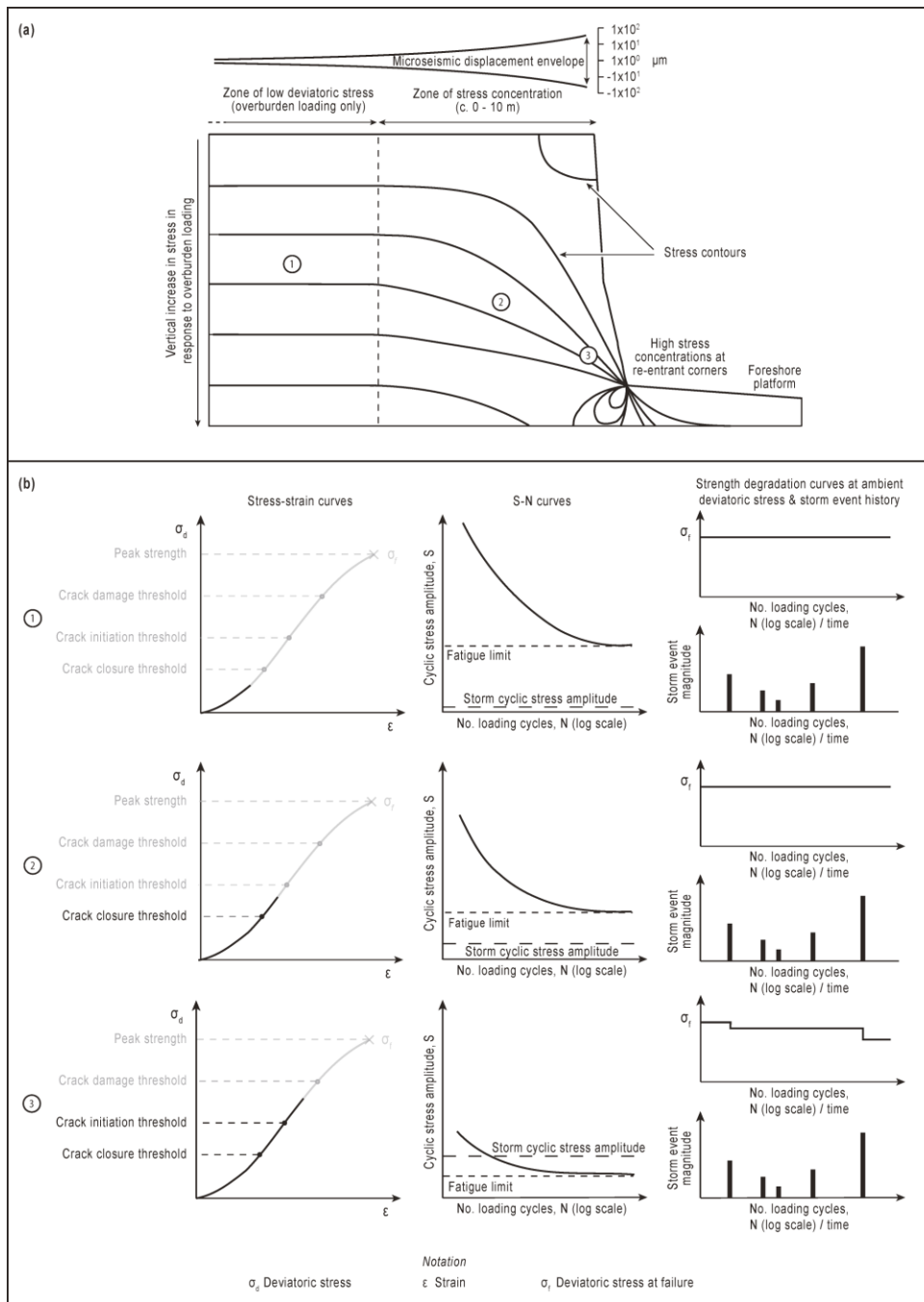
531 Reduced amplitude microseismic ground motions occurring during periods of relative  
532 quiescence between storm events may therefore be geomorphologically ineffective, and are  
533 physically unable to damage the rock. Curves of strength degradation against time may  
534 display stepped rather than continuous reductions in strength that are coincident only with  
535 rare displacement conditions during storms (Fig.s 3, 4 and 5). Episodic strength reduction  
536 contrasts starkly with the assumptions of the fatigue model proposed by Adams et al. (2005),  
537 which suggests that all microseismic displacements cause damage and rock weakening.

538 Whilst the combination of hydrographic and/or oceanographic controls on the occurrence of  
539 episodically damaging microseismic events is likely to be highly site specific, we consider it  
540 possible that such episodicity occurs at any site where frequently-experienced microseismic  
541 loading conditions are punctuated by ‘rare’ events that alter the magnitude and nature of  
542 ground motion. At our study site, we suggest that such conditions occur during high energy  
543 storm events. Elsewhere, such conditions may relate to extreme events that recur over a  
544 variety of timescales and result from, for example, regional tectonics and/or the occurrence of  
545 tropical storms.

#### 546 **4. Model of microseismic fatigue and damage accumulation**

547 A model is presented to describe our new interpretation of the spatial and temporal pattern of  
548 microseismic damage (Fig. 6) with reference to process zones that describe an hypothetical  
549 and idealised deviatoric stress distribution within a coastal rock cliff (cf. Wolters and Müller,  
550 2008). We do not explicitly consider the influence of discontinuities within the rock mass.  
551 This conceptual model is considered to be applicable to both jointed and homogeneous rock  
552 masses in terms of the processes and spatial distribution of microseismic damage. In jointed  
553 rock masses, however, we suggest that the processes of fatigue-induced strength degradation  
554 may operate along critically-stressed joints and fractures in addition to within the intact rock  
555 material (cf. Jafari et al., 2003). We consider three indicative key zones that describe  
556 susceptibility to microseismic damage accumulation, but we do not describe the exact form,  
557 extent or transition between zones; such characteristics are likely to be gradational and highly  
558 site-specific based on, for example, local geological, geomorphological and environmental  
559 conditions.

560



563 Fig. 6. Conceptual model of the spatial controls on the effectiveness of microseismic damage  
 564 and the potential episodic evolution of rock mass strength that occurs in response to high  
 565 energy (storm) loading conditions. (a) Summary of microseismic field conditions detailing  
 566 patterns of maximum observed microseismic amplitudes, an idealised deviatoric stress  
 567 distribution and the locations of process zones 1, 2 and 3 (see text for further explanation). (b)  
 568 Summary of potential stress state and damage conditions in zones 1, 2 and 3 and the potential  
 569 S-N and strength degradation curves that result from microseismic loading in these zones.  
 570

571 Zone 1 is located in the overburden stress loading zone, where deviatoric stresses are low and  
572 are insufficient to cause crack closure. Hence, microcrack densities are at background (prior  
573 to enhanced 'geomorphic' damage) levels. At this low deviatoric stress level, only a high  
574 number of high amplitude cycles operating around the mean stress are capable of causing  
575 failure in the rock, as demonstrated by the hypothetical S-N curve. At lower cyclic stress  
576 amplitudes, even very high numbers of loading cycles are insufficient to cause  
577 microfracturing and fatigue because the rock is insufficiently (pre-)damaged. The rock has a  
578 clear fatigue limit because cyclic stress amplitudes caused by microseismic displacement are  
579 lower than the fatigue limit. Hence, we suggest that there can be no reduction in strength as a  
580 result of microseismic cyclic loading.

581 Zone 2 is located within the zone of stress concentration, where deviatoric stresses begin  
582 closure of favourably-oriented microcracks. The rock is in an elastic deformation phase and  
583 the rock displays a definite fatigue limit. Despite slightly increased microseismic cyclic stress  
584 amplitudes, these are still not greater than the fatigue limit. Hence, there remains no reduction  
585 in strength as a result of microseismic cyclic loading.

586 Zone 3 is located within the damage accumulation zone of a pre-formed or incipient fracture  
587 resulting from gravitational failure. Here, deviatoric stress is at a level sufficient to initiate  
588 microcracking, though ambient static stresses are not sufficient to cause macroscale fracture;  
589 crack growth remains subcritical and stable (i.e. less than the crack damage threshold). This  
590 increased state of damage renders the rock more susceptible to lower cyclic stress amplitudes.  
591 The fatigue limit of the rock may now be less than the cyclic stress amplitudes occurring  
592 during storm events, allowing the microseismic displacements to accumulate damage,  
593 reducing rock strength such that it is more prone to fracture at lower deviatoric stresses. The



594 more frequent intervening lower magnitude displacements resulting from foreshore loading  
595 by ocean waves, for example, are unlikely to damage the rock due to the effects of crack tip  
596 blunting and residual stresses that close microcracks (Section 3.4.1). Although cyclic loading  
597 continues during non-storm conditions, we contend that these loading cycles do not damage  
598 the rock and there is no corresponding decrease in strength.

599 Hence, as suggested in the strength degradation curve, reductions in strength resulting from  
600 microseismic damage may be episodic, only occurring during high energy conditions that  
601 cause the previously experienced maximum dynamic microseismic stress to be exceeded.

## 602 **5. Discussion**

### 603 5.1 Geomorphic significance of microseismic ground displacements

604 By defining the likely spatial extent of damage accumulation zones and through consideration  
605 of the relative magnitude-frequency characteristics of microseismic ground displacements  
606 resulting from standard tidal loading effects and energetic storm conditions, we suggest that  
607 the likely opportunity for cyclic microseismic loading of coastal rock cliffs to cause damage  
608 and weakening through propagation and coalescence of microcracks is highly spatially and  
609 temporally restricted. Hence, as an isolated process, microseismic displacement may be  
610 unlikely to have sufficient opportunity to cause cumulative weakening of rock. This is  
611 particularly the case if cliff retreat rates are high relative to the net effect of microseismic  
612 damage processes, since a parcel of rock that slowly accumulates microseismic damage is  
613 likely to be exhumed, detached or eroded by other more ‘aggressive’ processes before  
614 microseismicity exerts a meaningful control on rock strength.

615 In reality, microseismic loading does not operate in isolation. Microseismic damage is part of  
616 a range of interacting, environmentally-controlled processes that can potentially effect  
617 subcritical crack growth and rock weakening (Pentecost, 1991; Main et al., 1993; Petley et  
618 al., 2005 a, b; Gómez-Heras et al., 2006; Hall et al., 2010; Gischig et al., 2011a, b; Smith et  
619 al., 2011). These processes act in synergy to increase microcrack density in a subcritical  
620 manner before coalescence occurs at a critical level, causing a transition from secondary to  
621 tertiary creep and, hence, an acceleration in crack growth rate that is no longer controlled by  
622 environmental forcing (Rosser et al., 2007). Microseismic ground displacements may only  
623 operate as an effective geomorphic agent, particularly as a preparatory weakening process (cf.  
624 Adams et al., 2005), as part of this suite of complementary processes.

## 625 5.2 Magnitude-frequency distribution of microseismic events

626 Our hypothesis that microseismic contributions to damage accumulation are episodic has  
627 significant implications for our understanding of the environmental controls on microseismic  
628 damage. We contend that environmental processes that cause greater displacements (such as  
629 storms) than those during standard loading conditions may result in solely tidally-controlled  
630 displacements being ineffective. Damage is contingent upon both the magnitude-frequency  
631 distribution of displacement and not solely magnitude alone. Consequently, inter-site  
632 comparison of displacement amplitudes in terms of damage and fatigue effects is unlikely to  
633 be meaningful without a full understanding of the full microseismic displacement and  
634 direction magnitude-frequency distributions at each site. This has important implications for  
635 the microseismic monitoring period itself; shorter duration monitoring periods lasting a few  
636 weeks, months or even years, are unlikely to capture the most damaging microseismic  
637 consequences. We advocate significantly longer monitoring campaigns tailored to the

638 recurrence of extremes (cf. Norman, 2012) to capture as much of the magnitude-frequency  
639 distribution and to better define what constitutes infrequent, highly damaging microseismic  
640 conditions.

### 641 5.3 Constraining the influence of microseismic damage on rockfall occurrence

642 Comparison of environmental (meteorological and oceanographic) processes with rockfall  
643 inventories at our study site has revealed few strong, statistically significant correlations  
644 (Rosser et al., 2007; Lim et al., 2010). This may result from the highly spatially specific and  
645 temporally restricted nature of microseismic damage potential and the temporal nature of  
646 fatigue microcrack growth.

647 Typically, attempts to correlate environmental processes with rockfall activity (the ultimate  
648 results of damage accumulation) are undertaken at relatively coarse temporal resolution  
649 (monthly, for example; cf. Rosser et al., 2007). Rock-damaging microseismic conditions  
650 (suitably-coincident magnitude and direction of displacement) occur infrequently but rapidly  
651 (over seconds) and at the microscale. Hence, comparison of time-averaged microseismic  
652 displacement data recorded at the cliff top with regional scale and time-averaged (hourly)  
653 oceanographic and/or meteorological datasets is unlikely to reveal the exact combination of  
654 environmental conditions required to cause microseismic damage. Greater temporal and  
655 spatial resolution of data describing environmental conditions may help to improve this  
656 linkage.

657 During the most damaging microseismic conditions (storms, for example), it is also likely  
658 that other processes conducive to damage and subsequent fracture, such as pore water  
659 pressure increases (Brooks et al., 2012), or ocean wave impact loading at the cliff base  
660 (Kirkgöz, 1990), also increase in magnitude and potential geomorphic effectiveness. Hence,

661 isolating the damage effect of each forcing variable becomes extremely difficult if not  
662 impossible in the field. This may further obscure any direct relationships between the  
663 development of fractures, manifest as rockfall activity, and microseismic loading.

664 Finally, if microcrack densities have evolved to a critical level, then a sufficiently large  
665 microseismic displacement episode may act as a catalyst for failure as critical strain  
666 thresholds are exceeded (Petley et al, 2005 a, b). Such an event is also not likely to be easily  
667 isolated or detected as the direct trigger mechanism of subsequent macro-scale fracture and  
668 rockfall activity, which requires an ‘internal’ self-organising yet highly time-dependent  
669 cascade of microcrack development and coalescence (Main et al., 1993). This process  
670 temporally separates cause from effect. The phenomenon of failure with no apparent direct  
671 environmental trigger has previously been recognised in monitoring datasets in coastal rock  
672 cliff environments (Rosser et al., 2007). Indeed, the microscale mechanical cracking  
673 processes that we propose conforms to the damage accumulation model developed by Rosser  
674 et al. (2007), which is based on temporal patterns of strain accumulation and rockfall within  
675 brittle coastal rock cliff materials.

## 676 **6. Conclusions**

677 By drawing together appropriate literature, theory and field data, we have reassessed the  
678 potential role that microseismic ground displacements may play in propagating  
679 microfractures and subsequently weakening rock masses via a cyclic loading and fatigue  
680 process. Our conclusions are:

- 681 1. Due to the low magnitude of the strains and resultant stresses generated, microseismic  
682 ground motions are likely to require rocks to undergo a critical level of stress and strain  
683 (i.e. a pre-damaged condition) before they can drive microcrack damage and fatigue. It is

684 suggested that such critical stressing occurs only in ‘damage accumulation zones’ of  
685 limited spatial extent, as governed by macroscale stress states, here shown in the near-  
686 cliff face stress concentration.

687 2. Microseismic ground displacements observed at our study site demonstrate low  
688 background amplitudes that display limited response to tide level. This relative  
689 quiescence in microseismic ground motion is interrupted by periods of greater  
690 displacement during energetic storm events. Higher amplitude displacements extend  
691 microcracks beyond conditions achievable by low amplitude background displacements,  
692 but by doing so cause blunting of microcrack tips and generate local residual stresses,  
693 which close the microcrack and curtail microcrack growth. The intervening and ongoing  
694 cyclic loading that occurs during non-storm events may therefore be insufficient to  
695 damage and weaken the rock mass.

696 3. At times of greatest displacement amplitude, our analysis demonstrates less frequent  
697 ground motions with a strong cliff normal component. These rarer displacements are  
698 likely to be more damaging, as they may cause a change in the microcrack tip stress  
699 distribution and separation mode and/or may cause interaction of microcrack populations  
700 that would not normally interact under standard (‘background’) loading conditions.

701 4. In response to the low frequency of occurrence of microseismic events that may damage  
702 rock, microseismic damage and strength degradation may occur episodically, rather than  
703 continuously in (quasi-)proportional and cumulative response to environmental forcing.

704 5. The necessary conditions for damage are highly restrictive, both spatially and temporally.  
705 Hence, we hypothesise that there is unlikely to be sufficient opportunity for microseismic  
706 ground motions to cause geomorphologically significant rock weakening, particularly  
707 when considered in the context of other processes in action. Whilst microseismic

708 displacements may, under suitable conditions, trigger changes in the rate of microcrack  
709 growth, elucidating the relationship between microseismic cause and rockfall effect is not  
710 straightforward.

## 711 **Acknowledgements**

712 This work was funded and supported by Cleveland Potash Ltd., which we gratefully  
713 acknowledge. We are also very grateful to the following: SEIS-UK for use of the  
714 microseismometers (NERC GEF loan 879) and for technical support and field assistance; NERC  
715 BIGF for GPS data; NERC BODC for oceanographic data; Peter Adams and Dave Milledge  
716 for sharing and discussing seismic data processing code; Chris Orton for assistance with  
717 drafting figures; Mike Lim and Sam Waugh for help during the fieldwork phase; Antony  
718 Long for helpful comments on an earlier draft of the manuscript; and Alex Densmore for  
719 useful discussions. We thank Adam Young and Mark Dickson for their detailed reviews of  
720 the manuscript and their helpful comments.

## 721 **References**

- 722 Adams, P. N., Anderson, R.S. and Revenaugh, J., 2002, Microseismic measurement of wave-  
723 energy delivery to a rocky coast. *Geology*, 30: 895-898.
- 724 Adams, P.N., Storlazzi, C.D. and Anderson, R.S., 2005. Nearshore wave-induced cyclical  
725 flexing of sea cliffs. *Journal of Geophysical Research*, 110, F02002.  
726 doi:10.1029/2004JF000217
- 727 Agar, R., 1960. Post-glacial erosion of the North Yorkshire Coast from the Tees Estuary to  
728 Ravenscar. *Proceedings of the Yorkshire Geological Society*, 32: 409–428.

729 Agliardi, F., Crosta, G. and Zanchi, A., 2001. Structural constraints on deep-seated slope  
730 deformation kinematics. *Engineering Geology*, 59: 83 – 102.

731 Allison, R.J., 1996. Stress and strain in geomorphology. In Mäusbacher, R. and Schulte, A.  
732 (eds). *Readings in Physical Geography*. Springer-Verlag, Heidelberg.

733 Anders, M. H. and Wiltschko, D.V., 1994. Microfracturing, paleostress and the growth of  
734 faults. *Journal of Structural Geology*, 16: 795–815.

735 Attewell, P.B. and Farmer, I.W., 1973. Fatigue behaviour of rock. *International Journal of*  
736 *Rock Mechanics and Mining Sciences*, 10: 1 – 9.

737 Barlow, J., Lim, M., Rosser, N., Petley, D. Brain, M., Norman, E. and Geer, M., 2012.  
738 Modeling cliff erosion using negative power law scaling of rockfalls. *Geomorphology* 139 –  
739 140: 416 – 424. doi:10.1016/j.geomorph.2011.11.006

740 Bieniawski, Z.T., 1967. Mechanism of brittle rock fracture. Part I: theory of the fracture  
741 process. *International Journal of Rock Mechanics and Mining Sciences and Geomechanics*  
742 *Abstracts*, 4: 395-406.

743 Bjerrum, L., 1967, Progressive failure in slopes of overconsolidated plastic clay and clay  
744 shales. *Journal of the Soil Mechanics and Foundations Division of the American Society of*  
745 *Civil Engineers*, 93: 1–49.

746 Brace, W.F., Paulding Jr., B.W. and Scholz, C., 1966. Dilatancy in the fracture of crystalline  
747 rocks. *Journal of Geophysical Research*, 71: 3939 – 3953. doi:10.1029/JZ071i016p03939

748 Brady, B.H.G. and Brown, E.T. 2004. Rock Mechanics for Underground Mining. Kluwer  
749 Academic Publishers, Dordrecht.

750 Brooks, S.M., Spencer, T. and Boreham, S., 2012. Deriving mechanisms and thresholds for  
751 cliff retreat in soft-rock cliffs under changing climates: Rapidly retreating cliffs of the Suffolk  
752 coast, UK. *Geomorphology*, 153 – 154: 48 – 60.

753 Cai, M., Kaiser, P.K., Tasaka, Y., Maejima, T., Morioka, H. and Minami, M., 2004.  
754 Generalized crack initiation and crack damage stress thresholds of brittle rock masses near  
755 underground excavations. *International Journal of Rock Mechanics & Mining Sciences*, 41:  
756 833 – 847.

757 Clarke, B.A. and Burbank, D.W., 2010. Bedrock fracturing, threshold hillslopes, and limits to  
758 the magnitude of bedrock landslides. *Earth and Planetary Science Letters*, 297, 577 – 586.  
759 doi:10.1016/j.epsl.2010.07.011

760 Clarke, B.A. and Burbank, D.W., 2011. Quantifying bedrock-fracture patterns within the  
761 shallow subsurface: Implications for rock mass strength, bedrock landslides, and erodibility.  
762 *Journal of Geophysical Research*, 116, F04009. doi: 10.1029/2011JF001987

763 Crawford, W. C., and Webb, S.C., 2000. Identifying and removing tilt noise from low-  
764 frequency (<0.1 Hz) seafloor vertical seismic data, *Bulletin of the Seismological Society of*  
765 *America*, 90: 952 – 963. doi: 10.1785/0119990121.

766 Dammeier, F., Moore, J.R., Haslinger, F. and Loew S., 2011.Characterization of alpine  
767 rockslides using statistical analysis of seismic signals. *Journal of Geophysical Research*, 116,  
768 F04024. doi:10.1029/2011JF002037



769 Deparis, J., Jongmans, D., Cotton, F., Baillet, L., Thouvenot, F. And Hantz, D., 2008.  
770 Analysis of Rock-Fall and Rock-Fall Avalanche Seismograms in the French Alps. Bulletin of  
771 the Seismological Society of America, 98: 1781 – 1796. doi: 10.1785/0120070082

772 Dickson, M.E. and Pentney, R., 2012. Micro-seismic measurements of cliff motion under  
773 wave impact and implications for the development of near-horizontal shore platforms.  
774 Geomorphology 151 – 152: 27 – 38. doi:10.1016/j.geomorph.2012.01.006

775 Dühnforth, M., Anderson, R.S., Ward, D and, Stock, G.M., 2010. Bedrock fracture control of  
776 glacial erosion processes and rates. Geology, 38, 423 – 426. doi: 10.1130/G30576.1

777 Eberhardt, E., Stead, D. and Stimpson, B., 1999. Quantifying progressive pre-peak brittle  
778 fracture damage in rock during uniaxial compression. International Journal of Rock  
779 Mechanics and Mining Sciences, 36: 361 – 380.

780 Eberhardt, E. Stead, D. and Coggan, J.S., 2004. Numerical analysis of initiation and  
781 progressive failure in natural slopes – the 1991 Randa rockslide. International Journal of  
782 Rock Mechanics and Mining Sciences, 41: 69 – 87.

783 Erarslan, N. and Williams, D.J., 2012a. Investigating the effect of cyclic loading on the  
784 indirect tensile strength of rocks. Rock Mechanics and Rock Engineering, 45: 327 – 340. doi:  
785 10.1007/s00603-011-0209-7

786 Erarslan, N. and Williams, D.J., 2012b. Mechanism of rock fatigue damage in terms of  
787 fracturing modes. International Journal of Fatigue, 43: 76 – 89.  
788 doi:10.1016/j.ijfatigue.2012.02.008

789 Faulkner, D.R., Mitchell, T.M., Healy, D. and Heap, M.J., 2006. Slip on 'weak' faults by the  
790 rotation of regional stress in the fracture damage zone. *Nature*, 444: 922-  
791 955. doi:10.1038/nature05353

792 Faulkner, D.R., Mitchell, T.M., Jensen, E., and Cembrano, J. 2011. Scaling of fault damage  
793 zones with displacement and the implications for fault growth processes. *Journal of*  
794 *Geophysical Research*, 116, B05403. doi:10.1029/2010JB007788

795 Giraud, A., Rochet, L. And Antoine, P., 1990. Processes of slope failure in crystallophyllian  
796 formations. *Engineering Geology*, 29: 241 – 253.

797 Gischig, V.S., Moore, J.R., Evans, K.F., Amann, F. and Loew, S., 2011a. Thermomechanical  
798 forcing of deep rock slope deformation: 1. Conceptual study of a simplified slope. *Journal of*  
799 *Geophysical Research*, 116, F04010. doi:10.1029/2011JF002006

800 Gischig, V.S., Moore, J.R., Evans, K.F., Amann, F. and Loew, S., 2011b. Thermomechanical  
801 forcing of deep rock slope deformation: 2. The Randa rock slope instability. *Journal of*  
802 *Geophysical Research*, 116, F04011. doi:10.1029/2011JF002007

803 Gómez-Heras, M., Smith, B.J. and Fort, R., 2006. Surface temperature differences between  
804 minerals in crystalline rocks: Implications for granular disaggregation of granites through  
805 thermal fatigue. *Geomorphology*, 78: 236 - 249.

806 Graizer, V., 2006. Tilts in strong ground motion, *Bulletin of the Seismological Society of*  
807 *America*, 96: 2090–2102. doi:10.1785/0120060065.

808 Gunzberger, Y., Merrien-Soukatchoff, V. and Guglielmi, Y., 2005. Influence of daily surface  
809 temperature fluctuations on rock slope stability: case study of the Rochers de Valabres slope

810 (France). *International Journal of Rock Mechanics and Mining Sciences*, 42: 331 – 349.  
811 doi:10.1016/j.ijrmms.2004.11.003

812 Hall, C., Hamilton, A., Woff, W.D., Viles, H.A. and Eklund, J.A., 2011. Moisture dynamics  
813 in walls: response to micro-environment and climate change. *Proceedings of the Royal*  
814 *Society A*, 467: 194-211 doi: 10.1098/rspa.20100131.

815 Heap, M.J., Baud, P. and Meredith, P.G., 2009. The influence of temperature on brittle creep  
816 in sandstones. *Geophysical Research Letters*, 36, L19305.doi:10.1029/2009GL039373

817 Heap, M.J., Faulkner, D.R., Meredith, P.G. and Vinciguerra, S., 2010. Elastic moduli  
818 evolution and accompanying stress changes with increasing crack damage: implications for  
819 stress changes around fault zones and volcanoes during deformation. *Geophysical Journal*  
820 *International*, 183: 225 – 236. doi: 10.1111/j.1365-246X.2010.04726.x

821 Hobbs, D.W., 1964. The tensile strength of rocks. *International Journal of Rock Mechanics*  
822 *and Mining Sciences*, 1: 385 – 396.

823 Hoek E. and Bieniawski Z.T., 1965. Brittle fracture propagation in rock under compression.  
824 *International Journal of Fracture Mechanics*, 1: 137 – 155.

825 Hsu, L., Finnegan, N.J. and Brodsky, E.E., 2011. A seismic signature of river bedload  
826 transport during storm events. *Geophysical Research Letters*, 38, L13407.  
827 doi:10.1029/2011GL047759, 2011

828 Jafari, M.K., Amini Hosseini, K., Pellet, F., Boulon, M. and Buzzi, O., 2003. Evaluation of  
829 shear strength of rock joints subjected to cyclic loading. *Soil Dynamics and Earthquake*  
830 *Engineering*, 23: 619 – 630.

831 Janssen, C., Wagner, F.C., Zang, A. and Dresen, G., 2001. Fracture process zone in granite:  
832 a microstructural analysis. *International Journal of Earth Sciences*, 90: 46–59.  
833 doi:10.1007/s005310000157

834 Janssen, M., Zuidema, J. and Wanhill, R. 2002. *Fracture Mechanics*. Spon Press/Taylor and  
835 Francis Group, London/New York.

836 Kirkgöz, M.S. 1990. An experimental investigation of a vertical wall response to breaking  
837 wave impact. *Ocean Engineering*, 17: 379 – 391.

838 Koons, P.O., Upton, P. and Barker, A.D. 2012. The influence of mechanical properties on the  
839 link between tectonic and topographic evolution. *Geomorphology*, 137 (1), 168 – 180.  
840 doi:10.1016/j.geomorph.2010.11.012

841 Kranz, R.L., 1983. Microcracks in rocks: a review. *Tectonophysics*, 100: 449 – 480.

842 Lajtai, E.Z., 1971. A theoretical and experimental evaluation of the Griffith theory of brittle  
843 fracture. *Tectonophysics*, 11:129 - 156.

844 Lavrov, A., Vervoort, A., Wevers, M., Napier, and Napier, J.A.L., 2002. Experimental and  
845 numerical study of the Kaiser effect in cyclic Brazilian tests with disk rotation. *International*  
846 *Journal of Rock Mechanics and Mining Sciences*, 39: 287 – 302.

847 Li, G., Moelle K.H. and Lewis, J.A., 1992. Fatigue crack growth in brittle Sandstones.  
848 *International Journal of Rock Mechanics and Mining Sciences and Geomechanics Abstracts*,  
849 2: 469 – 77.

850 Lim, M., Rosser, N., Allison, R. & Petley, D. 2010a. Erosional processes in the hard rock  
851 coastal cliffs at Staithes, North Yorkshire. *Geomorphology*, 114: 12 - 21.  
852 doi:10.1016/j.geomorph.2009.02.011

853 Lim, M., Rosser, N.J., Petley, D.N. and Keene, M, 2011. Quantifying the Controls and  
854 Influence of Tide and Wave Impacts on Coastal Rock Cliff Erosion. *Journal of Coastal*  
855 *Research*, 27: 46-56. doi:10.2112/JCOASTRES-D-09-00061.1

856 McLamore, R. and Gray, K.W., 1967. The mechanical behaviour of anisotropic sedimentary  
857 rocks. *Journal of Engineering for Industry, Transactions of the American Society of*  
858 *Mechanical Engineers, Series B*, 89: 62 – 76.

859 Main, I.G., Sammonds, P.R. and Meredith, P.G., 1993. Application of a modified Griffith  
860 criterion to the evolution of fractal damage during compressional rock failure. *Geophysical*  
861 *Journal International*, 115: 367–380. doi: 10.1111/j.1365-246X.1993.tb01192.x

862 Martin, C.D. and Chandler, N.A., 1994. The progressive fracture of Lac du Bonnet granite.  
863 *International Journal of Rock Mechanics and Mining Sciences and Geomechanics Abstracts*,  
864 31: 643 – 659.

865 Mitchell, T.M. and Faulkner, D.R., 2008. Experimental measurements of permeability  
866 evolution during triaxial compression of initially intact crystalline rocks and implications for  
867 fluid flow in fault zones. *Journal of Geophysical Research*, 113, B11412.  
868 doi:10.1029/2008JB005588, 2008

869 Molnar, P., Anderson, R.S. and Anderson, S.P., 2007. Tectonics, fracturing of rock, and  
870 erosion. *Journal of Geophysical Research*, 112, F03014. doi:10.1029/02005JF000433.

871 Moore, D. E. and Lockner, D.A., 1995. The role of microcracking in shear-fracture  
872 propagation in granite. *Journal of Structural Geology*, 17: 95 – 114.

873 Moore, J.R., Sanders, J.W., Dietrich, W.E. and Glaser, S.D., 2009. Influence of rock mass  
874 strength on the erosion rate of alpine cliffs. *Earth Surface Processes and Landforms*, 34: 1339  
875 – 1352. doi: 10.1002/esp.1821

876 Nasser, M.H.B., Grasselli, G. and Mohanty, B. 2010. Fracture Toughness and Fracture  
877 Roughness in Anisotropic Granitic Rocks. *Rock Mechanics and Rock Engineering*, 43: 403 –  
878 415. doi: 10.1007/s00603-009-0071-z

879 Ng, K-Y. And Petley, D.N., 2009. The use of pore pressure reinflation testing in landslide  
880 management in Hong Kong. *Quarterly Journal of Engineering Geology and Hydrogeology*,  
881 42: 487 - 498.

882 Niandou, H., Shao, J.F., Henry, J.P. and Fourmaintraux, D., 1997. Laboratory investigation of  
883 the mechanical behaviour of Tournemore Shale. *International Journal of Rock Mechanics  
884 and Mining Sciences*, 34: 3 – 16.

885 Norman, E.C. 2012. Microseismic monitoring of the controls on coastal rock cliff erosion.  
886 Unpublished PhD thesis, Durham University, UK. <http://etheses.dur.ac.uk/3586/>

887 Norman, E.C., Rosser, N.J., Brain, M.J., Petley, D.N. and Lim, M. In revision. Coastal cliff-  
888 top ground motions as proxies for environmental processes. *Journal of Geophysical Research*  
889 – Oceans.

890 Paterson, M.S., 1978. *Experimental Rock Deformation – the Brittle Field*. Springer, Berlin.

891 Peng, S. and Johnson, A.M., 1972. Crack growth and faulting in cylindrical specimens of  
892 Chelmsford granite. *International Journal of Rock Mechanics and Mining Sciences and*  
893 *Geomechanics Abstracts*, 9: 37 – 86.

894 Pentecost, A., 1991. The weathering rates of some sandstone cliffs, Central Weald, England.  
895 *Earth Surface Processes and Landforms*, 16: 83 - 91.

896 Petley, D.N., Higuchi, T., Petley, D.J., Bulmer, M.H. and Carey, J., 2005a. Development of  
897 progressive landslide failure in cohesive materials. *Geology*, 33: 201 – 204. doi:  
898 10.1130/G21147.1

899 Petley, D.N., Higuchi, T., Dunning, S., Rosser, N.J., Petley, D.J., Bulmer, M.H.K. and Carey,  
900 J.2005b. A new model for the development of movement in progressive landslides. In:  
901 Hungr, O., Fell, R., Couture, R. & Eberhardt, E. *Landslide Risk Management*. Balkema,  
902 Amsterdam.

903 Petley, D. N. & Petley, D. J., 2006. On the initiation of large rockslides: perspectives from a  
904 new analysis on the Vaiont movement record. In: Mugnozza, G., Strom, A. & Hermanns, R.  
905 L. (eds). *Massive Rock Slope Failure*. NATO. Rotterdam.

906 Potyondy, D.O., 2007. Simulating stress corrosion with a bonded-particle model for rock.  
907 *International Journal of Rock Mechanics and Mining Sciences*, 44: 677 – 691.  
908 doi:10.1016/j.ijrmms.2006.10.002

909 Rawson, P.F. and Wright, J.K., 2000. *The Yorkshire Coast*. The Yorkshire Coast Geologists'  
910 Association Guide No. 34. Geologists' Association, London.

911 Robinson, L.A. 1974. Towards a process response model of cliff retreat—the case of North  
912 East Yorkshire. Unpublished PhD thesis, University of Leeds, UK.

913 Rodgers, P. W., 1968. Response of horizontal pendulum seismometer to Rayleigh and love  
914 waves tilt and free oscillations of Earth. *Bulletin of the Seismological Society of America*,  
915 58: 1384 – 1406.

916

917 Rosser, N.J., Lim, M., Petley, D.N. and Dunning, S.A. 2007. Patterns of precursory rockfall  
918 prior to slope failure. *Journal of Geophysical Research*, 112, F04014.  
919 doi:10.1029/2006JF000642.

920 Roux. P-F, Marsan, D., Métaixian, J-P, O'Brien, G. and Moreau, L. 2008. Microseismic  
921 activity within a serac zone in an alpine glacier (Glacier d'Argentière, Mont Blanc, France).  
922 *Journal of Glaciology*, 54: 157 – 168. doi:10.3189/002214308784409053

923 Scholz, C.H., 1968. Microfracturing and inelastic deformation of rock in compression.  
924 *Journal of Geophysical Research*, 73: 1417 – 1432.

925 Smith, B.J., McCabe, S., McAllister, D., Adamson, C., Viles, H.A. and Curran, J.M., 2011. A  
926 commentary on climate change, stone decay dynamics and the 'greening' of natural stone  
927 buildings: new perspectives on 'deep wetting'. *Environmental Earth Sciences*, 63:1691–1700.  
928 Doi: 10.1007/s12665-010-0766-1

929 Stock, G.M., Martel, S.J., Collins, B.D. and Harp, E.L. 2011. Progressive failure of sheeted  
930 rock slopes: the 2009–2010 Rhombus Wall rock falls in Yosemite Valley, California, USA.  
931 *Earth Surface Processes and Landforms*, 37, 546 – 561. doi: 10.1002/esp.3192



- 932 Styles, T.D., Coggan, J.S. and Pine, R.J., 2011. Back analysis of the Joss Bay Chalk Cliff  
933 Failure using numerical modelling. *Engineering Geology*, 120: 81 – 90.  
934 doi:10.1016/j.enggeo.2011.04.004
- 935 Sunamura, T. 1992. *Geomorphology of Rocky Coasts*. John Wiley and Sons, Chichester.
- 936 Suresh, S., 1998. *Fatigue of Materials*. Cambridge University Press, Cambridge.
- 937 Tapponier, P. and Brace, W.F., 1976. Development of stress-induced microcracks in  
938 Westerly Granite. *International Journal of Rock Mechanics and Mining Sciences and*  
939 *Geomechanics Abstracts*, 13: 103 – 112.
- 940 Terzaghi, K., 1962. Stability of steep slopes on hard unweathered rock. *Géotechnique*, 12:  
941 251 – 270.
- 942 Tien Y.M., Lee D.H. and Juang C.H., 1990. Strain, pore pressure and fatigue characteristics  
943 of sandstone under various load conditions. *International Journal of Rock Mechanics and*  
944 *Mining Sciences and Geomechanics Abstracts*, 27, 283 – 289.
- 945 Tsai, V.C., Minchew, B., Lamb, M.P. and Ampuero, J-P., 2012. A physical model for seismic  
946 noise generation from sediment transport in rivers. *Geophysical Research Letters*, 39,  
947 L02404. doi:10.1029/2011GL050255
- 948 Vermilye, J. M. and Scholz, C.H., 1998. The process zone: A microstructural view of fault  
949 growth, *Journal of Geophysical Research*, 103: 12,223–12,237.

950 Vinciguerra, S., Trovato, C., Meredith, P.G. and Benson, P.M., 2005. Relating seismic  
951 velocities, thermal cracking and permeability in Mt. Etna and Iceland basalts, *International*  
952 *Journal of Rock Mechanics and Mining Sciences*, 42: 900 – 910.

953 Webb, S. C., and Crawford, W.C., 1999. Long-period seafloor seismology and deformation  
954 under ocean waves. *Bulleting of the Seismological Society of America*, 89: 1535 –  
955 1542. West, M.E., Larsen, C.F., Truffer, M., O’Neel, S. and LeBlanc, L., 2010. Glacier  
956 microseismicity. *Geology*, 38: 319 – 322. doi: 10.1130/G30606.1

957 Wilson, J. E., Chester, J.S. and Chester, F.M., 2003. Microfracture analysis of fault growth  
958 and wear processes, Punchbowl Fault, San Andreas System, California. *Journal of Structural*  
959 *Geology*, 25: 1855–1873.

960 Wolters, G. and Müller, G., 2008. Effect of cliff shape on internal stresses and rock slope  
961 stability. *Journal of Coastal Research*. 24: 43 – 50. <http://dx.doi.org/10.2112/05-0569.1>

962 Wyllie, D.C. and Mah, C., 2010. *Rock Slope Engineering: Civil and Mining*. Spon  
963 Press/Taylor and Francis Group, London/New York.

964 Xiao, J-Q, Feng, X-T, Ding, D-X and Jiang, F-L, 2011. Investigation and modeling on fatigue  
965 damage evolution of rock as a function of logarithmic cycle. *International Journal for*  
966 *Numerical and Analytical Methods in Geomechanics*, 35: 1127 – 1140. doi: 10.1002/nag.946

967 Young, A.P. and Ashford, S.A., 2008. Instability investigation of cantilevered seacliffs. *Earth*  
968 *Surface Processes and Landforms*, 33: 1661 – 1667. doi: 10.1002/esp.1636

- 969 Young, A.P., Adams, P.N., O'Reilly, W.C., Reinhard, E.F. and Guza, R.T., 2011. Coastal  
970 cliff ground motions from local ocean swell and infragravity waves in southern California.  
971 Journal of Geophysical Research, 116, C09007. doi:10.1029/2011JC007175
- 972 Young, A.P., Guza, R.T., Adams, P.N., O'Reilly, W.C. and Flick, R.E. Cross-shore decay of  
973 cliff top ground motions driven by local ocean swell and infragravity waves. Journal of  
974 Geophysical Research, 117. C06029. doi:10.1029/2012JC007908